Global prevalence of non-perennial rivers and streams

Mathis Loïc Messager, Bernhard Lehner, Charlotte Cockburn, Nicolas Lamouroux, Hervé Pella, Ton Snelder, Klement Tockner, Tim Trautmann, Caitlin Watt, T. Datry

Global prevalence of non-perennial rivers and streams
Main text

Mathis Loïc Messager [1, 2], Bernhard Lehner [1], Charlotte Cockburn [1, 3], Nicolas Lamouroux [2], Hervé Pella [2], Ton Snelder [4], Klement Tockner [5], Tim Trautmann [6], Caitlin Watt [1,7], Thibault Datry [2]

[1] Department of Geography, McGill University, 805 Sherbrooke Street West, Montreal, Quebec H3A 0B9, Canada
[2] RiverLY Research Unit, National Institute for Agricultural and Environmental Research (INRAE), 5 rue de la Doua, CS 20244, 69625 Villeurbanne Cedex, France
[3] Current affiliation: Department of Earth Science, Dartmouth College, Hanover, NH 03755, United States
[4] Unit 13, 212 Antigua Street, Christchurch 8023, New Zealand
[5] Senckenberg Society for Nature Research and Faculty of Biological Sciences, Goethe University Frankfurt, Frankfurt am Main, Germany
[6] Institute of Physical Geography, Goethe University Frankfurt, Frankfurt am Main, Germany
[7] Current affiliation: Lethbridge Research and Development Centre, Agriculture and Agri-Food Canada, 5403 1st Avenue South, Lethbridge, Alberta T1J 4B1, Canada

Corresponding authors: Mathis Loïc Messager (mathis.messager@mail.mcgill.ca), Bernhard Lehner (bernhard.lehner@mcgill.ca), Thibault Datry (thibault.datry@inrae.fr)

Summary

Flowing waters play a unique role in supporting global biodiversity, biogeochemical cycles, and human societies[1–5]. While the importance of permanent watercourses is well recognized, the prevalence, value and fate of non-perennial rivers and streams that periodically cease to flow tend to be overlooked, if not ignored[6–8]. This oversight contributes to the degradation of the main source of water and livelihood for millions of people[5]. Here we predict that water ceases to flow for at least one day per year along 51-60% of the world's rivers by length, demonstrating that non-perennial rivers and streams are the rule rather than the exception on Earth. Leveraging global information on the hydrology, climate, geology, and surrounding land cover of the Earth's river network, we show that non-perennial rivers occur within all climates and biomes, and on every continent. Our findings challenge the assumptions underpinning foundational river concepts across scientific disciplines[9]. To understand and adequately manage the world's flowing waters, their biodiversity and functional integrity, a paradigm shift is needed towards a new conceptual model of rivers that includes flow intermittence. By mapping the distribution of non-perennial rivers and streams, we provide a stepping-stone towards addressing this grand challenge in freshwater science.

Main

Virtually every river network on Earth includes channels that periodically cease to flow. From Himalayan snow-fed creeks to occasionally water-filled Saharan wadis, river flow cessation is naturally prevalent worldwide. Yet the global extent of intermittent rivers and ephemeral streams (IRES) is largely unknown. IRES vary widely in size and flow duration, encompassing all non-perennial watercourses — from large, rarely intermittent rivers with nearly continuous channel flow to mostly dry streams that only flow after intense rainfall (see **Extended Data Table 1** for additional definitions and IRES terminology). IRES are pivotal components of the landscape, significantly contributing to the biodiversity[1,2], biogeochemical processes and functional integrity of fluvial systems[3,4]. Many formerly perennial rivers and streams have become intermittent in the past 50 years due to water abstractions, climate change, and land use transitions, including sections of iconic rivers such as the Nile, Indus, Yellow, and Colorado[10,11]. Given continued global change, an increasingly large proportion of the global river network is expected to seasonally cease to flow over the coming decades[12,13].

Despite their prevalence, IRES are frequently mismanaged due to a lack of recognition[6], or altogether excluded from management actions and conservation laws[7]. As a result, non-perennial rivers and streams are being degraded at an alarming rate[6]. Recent attempts to further remove IRES from environmental legislation and national water governance systems (e.g., in the United States[8]), if implemented, would worsen their already inadequate protection. The long-standing neglect of IRES is partly the result of their continued omission from scientific research. Most freshwater science has focused on the functioning and conservation of perennial water bodies; and only recently has riverine flow cessation become a substantial subject of study[1,9,10]. Consequently, science-based methods for managing these unique ecosystems, such as biomonitoring tools and protocols, are still limited or absent[5,14].

Management frameworks also need to be adapted to conserve environmental flows in IRES[15] — i.e., the quantity, timing, and quality of freshwater flows necessary to sustain aquatic ecosystems and their associated benefits[16]. But perhaps the most important gap until now was our inability to quantify and map IRES worldwide. Accurate mapping of non-perennial rivers and streams would provide crucial baseline information to determine and monitor their role in biogeochemical and water cycles and in supporting global biological diversity[3].

Streamflow monitoring data for IRES are scant, spatially biased, and of uneven quality[17]. Indeed, most streamflow gauging stations are installed on large, perennial rivers worldwide[17]. The dearth of primary data has triggered the development of alternative methods to map IRES, including citizen science or expert field observations of streamflow state, *in-situ* sensor networks, and remote sensing[18–20]. However, these efforts only provide information at local scales and suffer from several limitations (e.g., remote sensing of smaller rivers can be obstructed by overhanging riparian vegetation and cloud cover[20]). Model-based classifications of river types, either IRES-focused (e.g., in mainland France[21], the north-western U.S.[22], eastern Australia[23]) or general (e.g., Australia[24], California[25]), have also provided important baseline estimates of the spatial distribution of IRES from the catchment to the national scale. However, a rigorous estimation of the global prevalence and distribution of IRES is still lacking.

In this study, we developed a statistical Random Forest (RF) model (see *Methods* for details) to produce the first reach-scale estimate of the distribution of IRES for the 23.3 million kilometres of mapped rivers and streams across the globe whose long-term average naturalised discharge exceeds 0.1 $m^3 s^{-1}$, and then extrapolated our IRES estimates to the nearly 64 million km of rivers and streams with an average discharge higher than 0.01 $m^3 s^{-1}$. For this purpose, we linked quality-checked observed streamflow data from 5,615 gauging stations (on 4,428 perennial and 1,187 non-perennial reaches) with 113 candidate

environmental predictors available globally (**Extended Data Table 2**). Predictors included variables describing climate, physiography, land cover, soil, geology, and groundwater as well as estimates of long-term naturalised (i.e., without anthropogenic water use in the form of abstractions or impoundments) mean monthly and mean annual flow (MAF), derived from a global hydrological model (WaterGAP 2.2[26]). Following model training and validation, we predicted the probability of flow intermittence for all river reaches in the RiverATLAS database[27], a digital representation of the global river network at high spatial resolution.

Prevalence and distribution of IRES

We predict that water ceases to flow for at least one day per year, on interannual average, along 41% of the mapped global river network length, i.e., all rivers and streams with MAF ≥ 0.1 $m^3 s^{-1}$ (**Fig. 1, Table 1**). However, any estimate of the percentage of IRES reaches in a river system, whether for a small catchment or for the globe, is inherently dependent on cartographic scale. Although many dryland rivers exhibit downstream decreases in discharge due to channel evaporation and transmission losses[28], river flow tends to become more permanent with increasing drainage area and distance from the headwaters in a basin[29], which is well reflected in the predictions of our model. Because of the dendritic nature of river networks, small headwater streams, which are more prone to intermittence, make up a greater proportion of the total stream length than larger downstream rivers[30]. Consequently, the percentage of the river network length that is non-perennial increases with decreasing size of the smallest mapped stream. To account for this distribution, we made a first-order approximation of the prevalence of intermittence in small streams by extrapolating our estimate to streams with 0.01 $m^3 s^{-1} \leq$ MAF < 0.1 $m^3 s^{-1}$ (see *Methods* for details). Including this size class, we estimate that 60% of all rivers and streams globally are IRES; and we found a lower bound of this estimate at 51% after applying an alternative, more

115 conservative extrapolation approach. This demonstrates, for the very first time, that IRES
116 represent the world's most widespread type of rivers.

117 For river flow to occur, water from rainfall, snowmelt, or releases from existing
118 storage (e.g., lakes, reservoirs, groundwater) must exceed losses from infiltration and
119 evapotranspiration[31]. Climatic variables, in particular climate-induced aridity, were therefore
120 the leading predictors of river flow cessation and the occurrence of IRES (**Fig. 2**). Our model
121 indicates that where evaporation rates significantly exceed precipitation for at least part of the
122 year, as expressed by a low aridity index (ratio of mean annual precipitation to mean annual
123 potential evapotranspiration), river networks comprise large proportions of IRES. In
124 extremely hot and xeric environments, which cover nearly a tenth of the global landmass and
125 encompass most of India, northern Australia and the Sahel region of Africa (see **Extended**
126 **Data Fig. 1a** for the global typology of bioclimates[32]), 95% of the river and stream network
127 length is prone to flow cessation (MAF ≥ 0.01 m^3 s^{-1}; **Table 1**). In these environments, we
128 find that even the main stem of major rivers, such as the Niger or Godavari, can dry out.

129 Outside of arid regions, flow in river networks is primarily controlled by catchment
130 processes influenced by interacting climate and basin conditions[1,29]. In cold climates, for
131 instance, a combination of scarce precipitation, its storage as snow during winter months, and
132 completely freezing streams[33] can lead to high prevalence of flow intermittence. In humid
133 and temperate regions, IRES are concentrated in the upper end of channel networks where
134 small drainage areas and steep slopes lead to rapid delivery of water to and through the river
135 channel, causing a lack of buffering from variations in precipitation[34]. Therefore, even in the
136 wettest climates (e.g., extremely hot and moist; **Extended Data Fig. 1a**), up to 35% of
137 headwater streams are non-perennial (**Table 1**). In lowland and large basins, temporary
138 storage and subsequent attenuated release from groundwater, lakes, and wetlands, as well as

139 the averaging of local hydrologic variability across a larger drainage area lead to more
140 balanced, steady, and thus perennial flow[29].

141 Our study is the first empirically grounded effort to specifically quantify the
142 prevalence of flow intermittence of rivers and streams globally, and to show that IRES occur
143 across all climates and biomes, and on every continent (**Fig. 1**, **Table 1**). Previous
144 assessments reported from 29% to 36% of the global length of rivers to be non-
145 perennial[28,36,37], with inferred and extrapolated estimates exceeding 50%[10,38]. However, these
146 estimates were either generalised hypotheses (e.g., based on the global distribution of
147 drylands[28]), geographically constrained (i.e., south of 60°N[36–38]), or research by-products
148 within larger projects (e.g., using a regional extrapolation to remove IRES from estimates of
149 the global CO_2 emissions of inland waters[38]), rather than dedicated global IRES
150 quantification efforts, and are therefore not directly comparable to our predictions. The FAO
151 AQUAMAPS[36] and GRIN[37] global river networks, for instance, assume that streamflow
152 cessation only occurs in arid and semi-arid areas. See Supplementary Information *Section I*
153 for a review of how previous estimates relate to our predictions, including a map of
154 AQUAMAPS and GRIN estimates.

155 Our study improves on these previous estimates because it represents diverse
156 hydrometeorological processes beyond aridity at the river reach scale (rather than at the basin
157 scale[38]) by leveraging extensive, high-resolution global data on the hydrology, climate,
158 physiography, geology, and surrounding land cover of the world's river network.
159 Furthermore, no global estimate prior to this study has used global empirical streamflow data
160 for training and validation, which allowed our model to make fine-grained predictions of the
161 intermittence class of rivers across all climates.

Model performance and uncertainties

Performance analysis showed that our RF model could predict the binary flow intermittence class of streamflow gauging stations with high confidence. Cross-validation yielded an overall classification accuracy (the percentage of correctly classified gauges), ranging from 90% to 92% (depending on cross-validation method), and indicated that model predictions were unbiased globally — i.e., adequately reflecting the proportion of IRES gauges in the training dataset. In general, sparsely gauged basins exhibit lower accuracy and higher bias (**Fig. 3**; e.g., in Africa and the Arctic). Boundary areas between climate zones (i.e., from mainly non-perennial regions to mainly perennial regions) are also characterized by higher misclassification rates (**Extended Data Fig. 2**). See **Fig. 3** as well as **Extended Data Table 3** for cross-validation results.

Our model is based on an inclusive definition of IRES as those rivers and streams that cease to flow at least one day per year on average. To test the sensitivity of our results to the specific threshold of cessation length, we adapted our model and found that 44-53% of the global river network cease to flow at least one month per year (lower-bound and main estimate, respectively, with MAF ≥ 0.01 m^3 s^{-1}; see *Methods*; **Extended Data Fig. 1b-c**).

Comparisons with national hydrographic datasets that include information on flow intermittence show that our model predicts a substantially higher prevalence of IRES in the contiguous U.S. than mapped in the country's atlas (by 31 percentage points), but coincides well with the patterns and extents depicted in the Australian, Argentinian, and Brazilian atlases, and with model-generated maps[39] in mainland France (**Extended Data Figs. 3-5**). The divergence observed in the U.S. (and to a limited extent in Australia) largely stems from the thresholds used to define IRES — when applying a minimum of one zero-flow month per year, our predictions more closely concur with the comparison dataset (**Extended Data Figs. 3 and 5**).

187 At an even more local scale, comparing our model predictions against datasets of
188 ground observation points of flow cessation for the U.S. Pacific Northwest and mainland
189 France reveals particular challenges in predicting flow intermittence for small rivers and
190 streams (median MAF ≈ 0.5 $m^3 s^{-1}$, **Extended Data Fig. 6**). Our model only achieved a
191 balanced accuracy of 0.59 for mainland France (n = 2,297) and of 0.47 for the U.S. Pacific
192 Northwest (n = 3,725), both under- and overestimating reported IRES, respectively. We
193 hypothesize that heavy water abstractions for domestic and agricultural use are the main
194 reason for the greater contemporary prevalence of intermittence observed in France[40] (from
195 2012 to 2019) than predicted by our model, which aims to depict the natural distribution of
196 IRES. In the U.S. Pacific Northwest, a lower frequency of observations per site may have led
197 to an underestimation of the prevalence of IRES in the comparison dataset, since the
198 probability of observing a no-flow event increases with the number of observations. In
199 addition, the mountainous landscape of the region is characterized by complex, local
200 hydrological processes associated with snow and groundwater dynamics that our model can
201 only superficially represent[22].
202 Despite the increasing uncertainties at national and local scales, the global validation
203 findings demonstrate that our overall statistics and large-scale representation of the spatial
204 distribution of IRES are robust. However, we advise caution in using our model outputs to
205 interpret fine-scale variations in intermittence for small spatial units or for small rivers and
206 streams. The quality of our model results is constrained by the resolution of the river network
207 and associated hydro-environmental predictor variables (250-1,000 m grid cells for most
208 predictors[27]). Accurate, fine-scale data on catchment soil types and lithology (e.g., karst
209 areas), riverbed sediments, and groundwater dynamics would be needed to capture variation
210 in the processes influencing flow intermittence at the sub-catchment and reach scales[29].
211 Groundwater–surface water interaction in particular is an enduring challenge in global

212 hydrological modelling[41] and represents a key process that is only partly represented in our
213 analysis. Also, potential local biases in training data (e.g., IRES being inconsistently
214 represented in streamflow gauging networks) introduce uncertainties. For instance, model
215 predictions in the south-eastern U.S. may overestimate the prevalence of IRES due to the
216 relative scarcity of gauging stations for model training on small, perennial watercourses in
217 that region. Similarly, the general under- and misrepresentation of small watercourses and
218 arid regions in the global hydrometric network[17] causes substantial difficulty in consistently
219 predicting the prevalence of IRES across the gamut of river types worldwide. Global
220 hydrological models are known to overestimate flow in arid climates[28], further complicating
221 IRES mapping in these regions.

222 Finally, our model's ability to predict the natural prevalence of flow intermittence is
223 affected by the impact of human activities on most gauged basins. Our study aims to depict
224 the natural distribution of non-perennial watercourses by excluding those gauging stations
225 from model training that were affected by flow regulation and/or whose flow intermittence
226 class changed over the discharge record (see *Methods*). We also used naturalised estimates of
227 discharge as predictor variables, which exclude anthropogenic water use in the form of
228 abstractions or flow regulation. Nevertheless, disentangling the potential effects of
229 contemporary land use, impoundments and human water abstractions on flow intermittence
230 remains a research frontier[42]. We expect that continued improvements in global hydro-
231 environmental datasets and hydrological models, combined with greater access to national
232 hydrometric datasets, will be key to improve future IRES mapping efforts.

233 **Understanding and managing IRES dynamics**

234 Our global map of IRES may become a crucial tool for understanding and managing these
235 long-undervalued ecosystems. High-resolution predictions of flow intermittence for all river
236 reaches with MAF ≥ 0.1 $m^3 s^{-1}$ can support spatially explicit studies down to the national

scale, while our first-order extrapolation of the total prevalence of non-perennial rivers and streams by region and river basin can offer additional insights into the role of IRES at continental and global scales. Our results also provide an important baseline for the assessment of future changes in flow intermittence in river networks. Quantifying the variability of flow cessation in space and time is required to better understand the impact of climate change, water abstraction and flow regulation; IRES are not only becoming increasingly common but the flow regime of existing IRES can shift e.g., from intermittent to ephemeral, whereas others will turn perennial[43].

In this study we identified *whether* and *where* rivers and streams cease to flow, but further quantification of the spatiotemporal dynamics of flow occurrence across stream networks worldwide is required to determine *when* and for *how long.* Knowledge of the natural frequency, duration, and timing of flow cessation, the primary determinants of the functioning of IRES[2,3], forms the basis of flow alteration analyses that can inform strategies to mitigate the impacts of future changes[15]. In particular, tools for assessing environmental flows globally are needed to appraise freshwater planetary boundaries[44] and to define quantitative targets for the 2030 UN Sustainable Development Goals[45]. Yet current tools exclude arid and semi-arid regions[46], which are dominated by IRES and where alternative sources of water are scarce[5].

Rethinking the significance of IRES

Our findings call for a paradigm shift in river science and management. The foundational concepts of river hydrology, ecology, and biogeochemistry have been developed from and for perennial waterways, and as a result, have all traditionally assumed year-round surface channel flow[9]. Here we show that this assumption is invalid for most rivers on Earth, which bolsters previous appeals for bringing together aquatic and terrestrial disciplines into river science[5,10].

Multiple conceptual models rely on the assumption that river discharge increases monotonically downstream from the headwaters to the mouth — e.g., the River Continuum Concept[47], a theoretical pillar of river ecology. Moreover, current models define hydrological connectivity within river networks in binary terms, as either free-flowing or perpetually fragmented by barriers such as waterfalls and dams[48], but we show that *temporary* fragmentation by seasonal drying[49] is a widespread phenomenon on Earth. In hydrology, the parameterization and calibration of predictive models of runoff and discharge are usually based on average or peak flows (e.g., for flood forecasting) rather than being calibrated to simulate low-flow quantities and timing, including flow cessation events, thus failing to reliably predict intermittence[20]. Up to date, global estimates of biodiversity have also overlooked IRES, which provide unique habitats for aquatic and terrestrial species[5,10]. Finally, recent research shows that omitting the role of non-perennial inland waters in carbon models may result in underestimating CO_2 emissions from inland waters by ~10%[4]; similar biases might undermine other global biogeochemical estimates, notably with respect to nitrogen cycling.

IRES have always been integral to human societies, whether culturally or as a source of food and water[5]. We estimate that for 52% of the world's population in 2020, the nearest river or stream is non-perennial (see *Methods*). The relationship between the seasonal hydrology of IRES and the ecosystems services they provide to society is a pressing area of research, particularly in regions where climate change is disrupting the water pulses to which people's livelihoods are tuned[50]. In many languages, multiple words exist to designate IRES and their mark on the landscape, highlighting the long history of inter-dependence between humans and seasonal freshwater systems[5]. However, the spiritual and cultural values that IRES provide, often to indigenous people (e.g., in Australia or in sub-Saharan Africa), remain to be acknowledged[5].

The past decade has witnessed several efforts to highlight both the values and ongoing degradation of IRES[6,8], yet current tools and policies still fall short of ensuring their biomonitoring and conservation[14,15]. A recognition of the prevalence and ecological significance of IRES by the scientific community may trigger efforts to adequately manage them and halt current attempts to exclude them from protective legislation[8]. As a stepping-stone, our new dataset intends to provide a baseline for identifying gaps in hydrological and biological monitoring efforts, to inform global biogeochemical upscaling and riverine species distribution models, and to decipher the links between hydrological patterns and culture-language. It can assist in discerning the role of IRES in the Earth system to safeguard the integrity of river networks and the well-being of those who directly rely on these ecosystems for their livelihood and culture.

References

1. Larned, S. T., Datry, T., Arscott, D. B. & Tockner, K. Emerging concepts in temporary-river ecology. *Freshw. Biol.* **55**, 717–738 (2010).
2. Leigh, C. & Datry, T. Drying as a primary hydrological determinant of biodiversity in river systems: a broad-scale analysis. *Ecography (Cop.).* **40**, 487–499 (2017).
3. Datry, T. *et al.* A global analysis of terrestrial plant litter dynamics in non-perennial waterways. *Nat. Geosci.* **11**, 497–503 (2018).
4. Marcé, R. *et al.* Emissions from dry inland waters are a blind spot in the global carbon cycle. *Earth-Science Rev.* **188**, 240–248 (2019).
5. Steward, A. L., von Schiller, D., Tockner, K., Marshall, J. C. & Bunn, S. E. When the river runs dry: human and ecological values of dry riverbeds. *Front. Ecol. Environ.* **10**, 202–209 (2012).
6. Acuña, V. *et al.* Why should we care about temporary waterways? *Science* (2014) doi:10.1126/science.1246666.
7. Fritz, K., Cid, N. & Autrey, B. Governance, legislation, and protection of intermittent rivers and ephemeral streams. in *Intermittent Rivers and Ephemeral Streams: Ecology and Management* 477–507 (Elsevier, 2017). doi:10.1016/B978-0-12-803835-2.00019-X.
8. Sullivan, S. M. P., Rains, M. C., Rodewald, A. D., Buzbee, W. W. & Rosemond, A. D. Distorting science, putting water at risk. *Science* **369**, 766–768 (2020).
9. Allen, D. C. *et al.* River ecosystem conceptual models and non□perennial rivers: A critical review. *WIREs Water* **7**, e1473 (2020).
10. Datry, T., Larned, S. T. & Tockner, K. Intermittent rivers: A challenge for freshwater ecology. *Bioscience* **64**, 229–235 (2014).
11. Ficklin, D. L., Abatzoglou, J. T., Robeson, S. M., Null, S. E. & Knouft, J. H. Natural and managed watersheds show similar responses to recent climate change. *Proc. Natl. Acad. Sci. U. S. A.* **115**, 8553–8557 (2018).
12. Jaeger, K. L., Olden, J. D. & Pelland, N. A. Climate change poised to threaten hydrologic connectivity and endemic fishes in dryland streams. *Proc. Natl. Acad. Sci.* **111**, 13894–13899 (2014).
13. Pumo, D., Caracciolo, D., Viola, F. & Noto, L. V. Climate change effects on the hydrological regime of small non-perennial river basins. *Sci. Total Environ.* **542**, 76–92 (2016).
14. Stubbington, R. *et al.* Biomonitoring of intermittent rivers and ephemeral streams in Europe: Current practice and priorities to enhance ecological status assessments. *Sci. Total Environ.* **618**, 1096–1113 (2018).
15. Acuña, V. *et al.* Accounting for flow intermittency in environmental flows design. *J. Appl. Ecol.* **57**, 742–753 (2020).
16. Arthington, A. H. *et al.* The Brisbane declaration and global action agenda on environmental flows (2018). *Front. Environ. Sci.* **6**, (2018).
17. Zimmer, M. A. *et al.* Zero or not? Causes and consequences of zero-flow stream gage readings. *Wiley Interdiscip. Rev. Water* **7**, e1436 (2020).
18. Beaufort, A., Lamouroux, N., Pella, H., Datry, T. & Sauquet, E. Extrapolating regional probability of drying of headwater streams using discrete observations and gauging networks. *Hydrol. Earth Syst. Sci.* **22**, 3033–3051 (2018).
19. Jaeger, K. L. & Olden, J. D. Electrical resistance sensor arrays as a means to quantify longitudinal connectivity of rivers. *River Res. Appl.* **28**, 1843–1852 (2012).
20. Yu, S. *et al.* Evaluating a landscape-scale daily water balance model to support spatially continuous representation of flow intermittency throughout stream networks. *Hydrol. Earth Syst. Sci.* **24**, 5279–5295 (2020).
21. Snelder, T. H. *et al.* Regionalization of patterns of flow intermittence from gauging station records. *Hydrol. Earth Syst. Sci.* **17**, 2685–2699 (2013).
22. Jaeger, K. L. *et al.* Probability of Streamflow Permanence Model (PROSPER): A spatially continuous model of annual streamflow permanence throughout the Pacific Northwest. *J. Hydrol. X* **2**, 100005 (2019).
23. Yu, S., Bond, N. R., Bunn, S. E. & Kennard, M. J. Development and application of predictive models of surface water extent to identify aquatic refuges in eastern Australian temporary stream metworks. *Water Resour. Res.* **55**, 9639–9655 (2019).
24. Kennard, M. J. *et al.* Classification of natural flow regimes in Australia to support environmental flow management. *Freshw. Biol.* **55**, 171–193 (2010).
25. Lane, B. A., Dahlke, H. E., Pasternack, G. B. & Sandoval□Solis, S. Revealing the diversity of natural hydrologic regimes in california with relevance for environmental flows applications. *JAWRA J. Am. Water Resour. Assoc.* **53**, 411–430 (2017).

26. Müller Schmied, H. *et al.* Sensitivity of simulated global-scale freshwater fluxes and storages to input data, hydrological model structure, human water use and calibration. *Hydrol. Earth Syst. Sci.* **18**, 3511–3538 (2014).
27. Linke, S. *et al.* Global hydro-environmental sub-basin and river reach characteristics at high spatial resolution. *Sci. data* **6**, 283 (2019).
28. Tooth, S. Process, form and change in dryland rivers: A review of recent research. *Earth Sci. Rev.* **51**, 67–107 (2000).
29. Costigan, K. H., Jaeger, K. L., Goss, C. W., Fritz, K. M. & Goebel, P. C. Understanding controls on flow permanence in intermittent rivers to aid ecological research: integrating meteorology, geology and land cover. *Ecohydrology* **9**, 1141–1153 (2016).
30. Benstead, J. P. & Leigh, D. S. An expanded role for river networks. *Nat. Geosci.* **5**, 678–679 (2012).
31. Godsey, S. E. & Kirchner, J. W. Dynamic, discontinuous stream networks: Hydrologically driven variations in active drainage density, flowing channels and stream order. *Hydrol. Process.* **28**, 5791–5803 (2014).
32. Metzger, M. J. *et al.* A high-resolution bioclimate map of the world: a unifying framework for global biodiversity research and monitoring. *Glob. Ecol. Biogeogr.* **22**, 630–638 (2013).
33. Tolonen, K. E. *et al.* Parallels and contrasts between intermittently freezing and drying streams: From individual adaptations to biodiversity variation. *Freshw. Biol.* **64**, 1679–1691 (2019).
34. Prancevic, J. P. & Kirchner, J. W. Topographic controls on the extension and retraction of flowing streams. *Geophys. Res. Lett.* **46**, 2084–2092 (2019).
35. Nembrini, S., König, I. R. & Wright, M. N. The revival of the Gini importance? *Bioinformatics* **34**, 3711–3718 (2018).
36. FAO. AQUAMAPS: Global spatial database on water and agriculture. https://data.apps.fao.org/aquamaps/ (2014).
37. Schneider, A. *et al.* Global-scale river network extraction based on high-resolution topography and constrained by lithology, climate, slope, and observed drainage density. *Geophys. Res. Lett.* **44**, 2773–2781 (2017).
38. Raymond, P. A. *et al.* Global carbon dioxide emissions from inland waters. *Nature* **503**, 355–359 (2013).
39. Snelder, T. H. *et al.* Regionalization of patterns of flow intermittence from gauging station records. *Hydrol. Earth Syst. Sci.* **17**, 2685–2699 (2013).
40. Tramblay, Y. *et al.* Trends in flow intermittence for European rivers. *Hydrol. Sci. J.* **66**, 37–49 (2021).
41. Döll, P., Douville, H., Güntner, A., Müller Schmied, H. & Wada, Y. Modelling freshwater resources at the global scale: challenges and prospects. *Surv. Geophys.* **37**, 195–221 (2016).
42. Hammond, J. C. *et al.* Spatial patterns and drivers of nonperennial flow regimes in the contiguous United States. *Geophys. Res. Lett.* **48**, (2021).
43. Döll, P. & Schmied, H. M. How is the impact of climate change on river flow regimes related to the impact on mean annual runoff? A global-scale analysis. *Environ. Res. Lett.* **7**, 014037 (2012).
44. Gleeson, T. *et al.* The water planetary boundary: interrogation and revision. *One Earth* **2**, 223–234 (2020).
45. Dickens, C. *et al. Incorporating environmental flows into "water stress" indicator 6.4.2 - guidelines for a minimum standard method for global reporting*. https://cgspace.cgiar.org/handle/10568/99257 (2019).
46. Sood, A. *et al. Global environmental flow information for the sustainable development goals*. vol. 168 (2017).
47. Vannote, R. L., Minshall, G. W., Cummins, K. W., Sedell, J. R. & Cushing, C. E. The river continuum concept. *Can. J. Fish. Aquat. Sci.* **37**, 130–137 (1980).
48. Grill, G. *et al.* Mapping the world's free-flowing rivers. *Nature* **569**, 215–221 (2019).
49. Stanley, E. H., Fisher, S. G. & Grimm, N. B. Ecosystem expansion and contraction in streams: Desert streams vary in both space and time and fluctuate dramatically in size. *Bioscience* **47**, 427–435 (1997).
50. Datry, T. *et al.* Flow intermittence and ecosystem services in rivers of the Anthropocene. *J. Appl. Ecol.* **55**, 353–364 (2018).

Tables

Table 1. Global prevalence of IRES across climate zones and streamflow size classes.

Climate zone[1]	Prevalence of intermittence (% of network length) by streamflow size class ($m^3 s^{-1}$)							Total intermittence % length	Total stream length[2] 10^3 km
	extrapolated[3] *$[10^{-2},10^{-1})$*	mapped $[10^{-1},1)$	$[1,10)$	$[10,10^2)$	$[10^2,10^3)$	$[10^3,10^4)$	$\geq 10^4$	including | (excluding) extrapolated stream class[3]	
Extremely hot and arid	*100*	100	100	98	49	0	-	99 | (98)	1032 | (249)
Hot and arid	*100*	100	100	97	46	0	-	99 | (98)	990 | (238)
Arctic 1	*100*	92	71	100	-	-	-	96 | (92)	11 | (6)
Warm temperate and xeric	*99*	96	89	59	11	0	0	96 | (89)	1351 | (444)
Extremely cold and wet 2	*100*	93	69	34	0	-	-	96 | (87)	766 | (243)
Extremely hot and xeric	*99*	90	95	90	45	0	0	95 | (89)	4551 | (1,605)
Arctic 2	*100*	89	18	8	-	-	-	92 | (82)	98 | (41)
Cool temperate and xeric	*94*	81	70	37	2	0	-	87 | (72)	1709 | (552)
Extremely cold and mesic	*96*	70	45	34	26	22	0	83 | (61)	8083 | (3,051)
Extremely cold and wet 1	*92*	59	10	1	0	-	-	72 | (50)	227 | (109)
Cold and mesic	*90*	47	26	6	3	0	0	70 | (37)	8189 | (3,084)
Warm temperate and mesic	*84*	45	35	16	1	0	0	63 | (39)	3582 | (1,646)
Hot and dry	*77*	47	36	23	7	0	0	62 | (41)	4054 | (1,683)
Cool temperate and dry	*65*	46	34	11	0	0	0	57 | (39)	4087 | (1,325)
Hot and mesic	*77*	30	24	23	5	0	0	54 | (27)	4452 | (2,023)
Extremely hot and moist	*35*	18	20	21	4	0	0	30 | (18)	19117 | (6,002)
Cool temperate and moist	*52*	18	10	0	0	0	-	29 | (13)	1164 | (691)
Cold and wet	*34*	1	0	0	0	0	-	14 | (1)	493 | (299)
World	***70***	**47**	**35**	**26**	**9**	**1**	**0**	**60 | (41)**	**63,956 | (23,291)**

[1] Global Environmental Stratification (GEnS)[32], see **Extended Data Fig. 1a**.
[2] Excluding sections of river reaches contained within a lake.
[3] Extrapolated statistics based on the main estimate (as opposed to the lower-bound estimate, see *Methods* for details).

Figure legends

Figure 1. Global distribution of non-perennial rivers and streams. [Alternative title: Non-perennial rivers and streams occur in all climates, biomes, and continents.]

Intermittence is defined as flow cessation for at least one day per year on average. The median probability threshold of 0.5 was used to determine the binary flow intermittence class for each reach in RiverATLAS[27]. Mapping software: ArcMap™ (ESRI).

Figure 2. Climate-induced aridity and hydrologic variables are the main predictors of global flow intermittence.

The two sets of ranked predictor variables represent results from a split random forest model trained on **a**, gauges with a mean annual naturalised flow < 10 $m^3 s^{-1}$ and **b**, gauges with a mean annual naturalised flow ≥ 1 $m^3 s^{-1}$. See *Methods – Machine learning models* for details on model structure and implementation. Rectangular bars show the balanced accuracy-weighted average of Actual Impurity Reduction[35] (AIR) across non-spatial cross-validation folds and repetitions. The longer the bar (i.e., the higher the AIR), the more important the variable in predicting flow intermittence. Error brackets show ± one weighted standard deviation of AIR. After the variables' names, the first abbreviation denotes each variable's spatial extent: *p* (derived at the pour point of the river reach), *c* (derived within the local catchment that drains directly into the reach), or *u* (derived within the total drainage area upstream of the reach pour point). The second abbreviation denotes each variable's dimension: yr (annual average), mn (annual minimum), mx (annual maximum), or mj (spatial majority). See *Methods* and **Extended Data Table 2** for data sources of variables.

Figure 3. Flow intermittence classification accuracy decreases and prediction bias increases in river basins with fewer streamflow gauging stations.

Maps of **a**, classification accuracy, **b**, prediction bias, and **c**, number of streamflow gauging stations per river basin based on 40-fold spatial cross-validation. See Supplementary Information **Fig. S3** for the distribution of cross-validation folds. River basins correspond to BasinATLAS[27] level 3 subdivisions with an average surface area of 4.6 x 10^5 km^2. Mapping software: ArcMap™ (ESRI).

Methods

See **Extended Data Fig. 7** for a summary of the data and methods used in this study.

Data

Global underpinning hydrography

We predicted the distribution of IRES for river reaches in the global RiverATLAS database[27]. RiverATLAS is a widely-used representation of the global river network built on the hydrographic database HydroSHEDS[51,52]. Rivers are delineated based on drainage direction and flow accumulation maps derived from elevation data at a pixel resolution of 3 arc-seconds (~90 m at the equator) and subsequently upscaled to 15 arc-seconds (~500 m at the equator). In this study, we only included river reaches with a modelled MAF ≥ 0.1 m^3 s^{-1} and excluded i) smaller streams (due to increasing uncertainties in their geospatial location and flow estimates derived from global datasets and models; see also *Hydro-environmental predictor variables* below); and ii) sections of river reaches within lakes (identified based on HydroLAKES polygons[53]). We define a 'river reach' as a cartographic — rather than a functional — unit, represented by the smallest spatial element of our global river network, that is, a line segment between two neighbouring confluences. We made predictions for 6,198,485 individual river reaches with an average length of 3.8 km, totalling 23.3 million kilometres of river network.

Reference intermittence data for model training and cross-validation

Two streamflow gauging station repositories were used as the source of training and cross-validation data for the split Random Forest (RF) model (**Extended Data Fig. 7b-8**) — the World Meteorological Organization Global Runoff Data Centre (GRDC)[54] database ($n \approx$ 10,000) and a complementary subset of the Global Streamflow Indices and Metadata archive (GSIM, $n \approx 31{,}000$), a compilation of twelve free-to-access national and international streamflow gauging station databases[55]. Whereas the GRDC offers daily river discharge

values for most stations, GSIM only contains time series summary indices computed at the yearly, seasonal and monthly resolution (calculated from daily records whose open-access release is restricted for some of the compiled data sources)[56]. Therefore, we used the GRDC database as the core of our training/testing set and complemented it with a subset of streamflow gauging stations from GSIM. A GSIM station was included only if i) it was not already part of the GRDC database, ii) it included auxiliary information on the drainage area of the monitored reach (for reliably associating it to RiverATLAS), iii) it had a drainage area < 100 km^2 or else (i.e., for gauges with drainage area ≥ 100 km^2) it was located either iv) on an IRES or v) in a river basin which did not already contain a GRDC station (assessed based on level 5 sub-basins of the global BasinATLAS database[51], average sub-basin area = 2.9 x 10^4 km^2). We applied the described GSIM selection criteria to balance the relative amount of non-perennial vs. perennial records, and the spatial distribution of stations in the model training dataset.

Each station in the combined dataset was geographically associated with a reach in the RiverATLAS stream network and every discharge time series was quality-checked through statistical and manual outlier detection (see Supplementary Information *Section II - Selection and pre-processing of gauging station and discharge data* for details on these procedures). Non-perennial gauging stations were only included in the dataset if they were free of anomalous zero-flow values (e.g., from instrument malfunction, gauge freezing, tidal flow reversal[17]). We also excluded stations whose streamflow was potentially dominated by reservoir outflow regulation (i.e., with a degree of regulation > 50%[27,57]) or whose discharge time series exhibited an alteration (see online research compendium at https://messamat.github.io/globalIRmap/ for an interactive visualization of processing information for every gauging station) as flow regulating structures may change the flow class of a river either from perennial to non-perennial or vice-versa depending on their mode

and rules of operation[58,59]. We further narrowed our selection by adding only gauging stations with a streamflow time series spanning at least 10 years — excluding years with more than 20 days of missing records for the calculation of this criterion and in subsequent analysis. Finally, we classified stations as non-perennial if their recorded discharge dropped to zero at least one day per year on average over the years of record, and as perennial otherwise. Stations with at least one zero-flow day per year on average (i.e., non-perennial) but without a zero-flow day during 20 consecutive valid years of data (those with ≤ 20 missing days), anywhere in their record, were deemed either to have experienced a shift in flow intermittence class (regardless of the direction of the shift) or to have ceased to flow due to exceptional conditions of drought and were also excluded. Based on these selection criteria, the training dataset contained data for 4,428 perennial river reaches and for 1,187 non-perennial reaches, with 41 and 34 years of daily streamflow data on average, respectively, across all continents (except Antarctica) (**Extended Data Fig. 8**).

The threshold used to define flow intermittence varies among studies, ranging from a single zero-flow day across the entire streamflow record[21,60] to at least five days per year on average[61]. Because zero-flow values in streamflow gauging records may be erroneous[17], other studies have used a flow percentile threshold value (e.g., Q99 < 0.0283 $m^3 s^{-1}$ in the U.S. Pacific Northwest[22]). To test the sensitivity of altering our criterion (one zero-flow day per year on average) on the resulting number of non-perennial stations, we changed the threshold to one zero-flow month (30 consecutive or non-consecutive days) per year, which yielded a dataset with 4,735 perennial stations and 880 non-perennial stations, respectively. Given the substantial difference between these thresholds, we also produced model estimates for the latter definition (**Extended Data Fig. 1b-c**).

Although our training dataset of gauging stations encompasses a wide range of river types found on Earth, it is inherently limited by the global availability of hydrometric data

(**Extended Data Fig. 8**). Most notably, rivers with MAF > 500 $m^3 s^{-1}$ are over-represented whereas those with MAF < 50 $m^3 s^{-1}$ are under-represented. In addition, few stations monitor rivers in extreme climates, whether cold or hot, dry or wet (e.g., classes 1-4 and 16-18 for extremely cold and extremely hot climates, respectively; **Extended Data Fig. 1a** shows the extent of each climate stratum[32]). Other significantly under-represented river types include those with annual average snow cover extent > 75% in their upstream drainage area and rivers with a shallow groundwater table or with > 90% of karst outcrops across their upstream drainage area.

Hydro-environmental predictor variables

The primary source of predictor variables was the global RiverATLAS database, version 1.0, which is a subset of the broader HydroATLAS product[27]. RiverATLAS provides hydro-environmental information for all rivers of the world, both within their contributing local reach catchment and across the entire upstream drainage area of every reach (**Extended Data Table 2**). This information was derived by aggregating and reformatting original data from well-established global digital maps, and by accumulating them along the drainage network from headwaters to ocean outlets[27].

RiverATLAS also includes estimates of long-term (1971-2000) naturalised (i.e., without anthropogenic water use in the form of abstractions or impoundments) mean monthly and mean annual flow (MAF). These discharge estimates are derived through a geospatial downscaling procedure[51] based on the 0.5 degree resolution runoff and discharge layers provided by the global WaterGAP model (version 2.2 as of 2014[26]). A validation of the downscaled discharge estimates against observations at the 2,131 GRDC gauging stations used in this study with ≥ 20 years of streamflow data from 1971 to 2000, representing rivers with MAF between 0.006 and 180,000 $m^3 s^{-1}$, confirmed good overall correlations for MAF (log-log least-square regression, $R^2 = 0.96$, with a symmetric mean absolute percentage error

545 sMAPE of 30%; see Supplementary Information **Table S1** for all validation results). The
546 sMAPE increased from 5% for rivers with MAF ≥1000 $m^3 s^{-1}$ to 20% for 10 $m^3 s^{-1}$ ≤ MAF
547 <1000 $m^3 s^{-1}$, and to 52% for MAF < 10 $m^3 s^{-1}$. Minimum monthly discharge was also found
548 to be an effective proxy for Q90 (R^2=0.84).

549 We complemented the RiverATLAS v1.0 data with three additional sets of variables.
550 The first set of variables describes the inter-annual open surface water dynamics as
551 determined by remote sensing imagery from 1999 to 2019[62]. In the original dataset, each 30-
552 meter resolution pixel which has been covered by water sometime during this time period
553 was assigned one of seven "interannual dynamic classes" (e.g., permanent water, stable
554 seasonal, high frequency changes) based on a time series analysis of the annual percent of
555 open water in the pixel. We computed the percent coverage of each of these interannual
556 dynamic classes relative to the total area of surface water within the contributing local
557 catchment and across the entire upstream drainage area of every river reach.

558 Second, we replaced the soil and climate characteristics in RiverATLAS v1.0 with
559 updated datasets. Specifically, we computed the average texture of the top 100 cm of soil
560 based on SoilGrids250m version 2[63]. We also updated the climate variables with WorldClim
561 version 2[64] (adding all bioclimatic variables to the existing set of variables) as well as the
562 Global Aridity Index and Global Reference Evapotranspiration (Global-PET) datasets version
563 2[65]. Finally, we updated the Climate Moisture Index (CMI), computed from the annual
564 precipitation and potential evapotranspiration datasets provided by the WorldClim v2 and
565 Global-PET v2 databases, respectively.

566 We derived a third set of variables by combining multiple variables already included
567 in the model through algebraic operations. These metrics included the runoff coefficient (i.e.,
568 ratio of MAF and mean annual precipitation), specific discharge (i.e., MAF per unit drainage
569 area), and various temporal (e.g., minimum annual/maximum annual discharge) and spatial

570 (e.g., mean elevation in local reach catchment/mean elevation in upstream drainage area)
571 ratios.

572 The application of all described procedures yielded a total of 113 candidate predictor
573 variables to be used in our statistical model development (**Extended Data Table 2**).

574 **Machine learning models**

575 We developed and used a split RF machine learning model to predict the flow
576 intermittence class, as a probability response, of all river reaches globally, with 1 denoting a
577 100% predicted probability of being an IRES. RF models have already been successfully
578 used to predict the distribution of IRES in Australia and France[21,66] and they have been
579 shown to achieve high performance when compared to other approaches, including other
580 machine learning models, logistic regression, and single decision trees[67,68]. Below, we briefly
581 describe the model development and validation procedure conducted for our split RF model;
582 see Supplementary Information *Section III - Random forest implementation* for additional
583 information.

584 Our final predictions are based on the probability RF algorithm developed by Malley
585 and colleagues[69], a derivative of the standard RF algorithm for making probabilistic
586 predictions of class membership, as included in the *ranger* R package[70]. This algorithm was
587 selected following a comparison[71,72] of several probability RF variants (namely, Conditional
588 Inference Forest[73,74] and a newly developed regression RF algorithm using MAXimally
589 selected rank STATistics[75]). To address known biases in RF models from class imbalance in
590 the training data (more perennial than non-perennial gauging stations on large rivers)[22,76], we
591 implemented random oversampling of non-perennial gauging stations[77].

592 For our split model approach, we trained and cross-validated two probability RF sub-
593 models with slightly overlapping ranges in river size, one trained to predict the streamflow
594 intermittence probability of small-to-medium rivers with MAF < 10 $m^3 s^{-1}$ and the other for

595 medium-to-large rivers with MAF ≥ 1 $m^3 s^{-1}$. Within the overlapping range of 1-10 $m^3 s^{-1}$
596 MAF, the average probability was calculated to avoid abrupt transitions at a singular size
597 threshold. This split approach performed better than a single model and was motivated by the
598 distinct class imbalance in training gauging stations between large rivers (4.87:1 perennial to
599 non-perennial ratio) versus small rivers (1.98:1 perennial to non-perennial ratio). With a
600 single model, the use of a common oversampling factor for both size classes underpredicted
601 the prevalence of IRES in large rivers (see **Extended Data Table 3**).

602 **Model development and diagnostics**

603 To optimize the predictive performance of the two sub-models, avoid overfitting, and
604 obtain unbiased estimates of statistical uncertainty, we implemented a nested resampling
605 framework for hyperparameter tuning and cross-validation[78], first for comparison across RF
606 algorithm variants, and then for comparing model performance with and without predictor
607 variable selection (see Supplementary Information *Section IV - Model development and*
608 *diagnostics: technical documentation* for a full description of the tuning and cross-validation
609 procedure[79,80]). Tuning was performed for 2-3 hyperparameters (depending on the RF
610 algorithm) through random search with a termination criterion of 100 iterations. The inner
611 (hyperparameter tuning) loop was composed of a 4-fold cross-validation and the outer loop
612 (for predictive performance assessment) involved a twice-repeated 3-fold cross-validation.
613 Cross-validation strategies usually involve 2-10 folds[79], with a lower number of folds (as
614 chosen here) yielding a more stringent evaluation of performance (i.e., a relatively
615 pessimistic evaluation bias). The outer cross-validation procedure was repeated twice and the
616 results were averaged to reduce the variance caused by randomly splitting the data into few
617 folds[78]. A spatial cross-validation procedure based on *k*-means spatial clustering (*k*=40, see
618 Supplementary Information **Fig. S3** for the distribution of clusters) was also used in the outer
619 resampling loop to avoid overoptimistic error estimates that arise in cases of significant

spatial autocorrelation[81–84]. We chose to implement 40 spatial folds to strike a balance between two extremes. Fewer folds would risk evaluating the predictive ability of the model across areas so large that they may represent unique hydro-climatic conditions outside of the model's training set (for a given fold), therefore underestimating the model's performance. More folds would have inflated our estimate of model accuracy by relying on training sets too similar to the testing sets and would have made the computational requirements of cross-validation even greater.

All algorithms were compared using the same inner and outer sets of training and testing partitions. Hyperparameters were tuned to optimize the Balanced class ACCuracy (BACC) metric[85], which is equivalent to the raw accuracy (or one minus the misclassification rate) but with each sample weighted according to the inverse prevalence of its true class (large river model: 4.87 and 1.00 weights for the non-perennial and perennial classes, respectively; small river model: 1.98 and 1.00 for the non-perennial and perennial classes, respectively). To assess predictor variable importance, weighted averages of Actual Impurity Reduction (AIR, an unbiased version of Gini impurity[35]) and the associated *p*-values (determined via 100 permutations, following ref[86]) were computed for each outer resampling cross-validation fold and repetition, using the BACC of each resampling instance as weight.

Prior to final model training and evaluation, only predictors with a variable importance *p*-value < 0.05 were retained, so that 92 and 82 variables were retained in the final small-river and large-river models, respectively. Variable selection was implemented to both increase model performance[87,88] and decrease model training time.

In addition to the BACC and the variable importance, several additional diagnostics were examined to determine the performance and characteristics of the RF model as follows:

(i) We assessed the classification accuracy (percentage of correctly classified gauges), the sensitivity (percentage of correctly classified IRES reaches, also

known as true positive rate or recall), specificity (percentage of correctly classified perennial reaches, also known as true negative rate or selectivity), and precision (percentage of reaches predicted to be IRES that are actually IRES) of the model for each streamflow size class (**Extended Data Table 3**), based on spatial and non-spatial cross-validations.

(ii) We examined the geographic, hydrological, and environmental distributions of the intermittence prediction residuals (IPR) for each reference stream gauging station (**Extended Data Fig. 2**):

IPR = predicted intermittence probability – observed intermittence class (Equation 1), with observed intermittence class IR = {0: perennial, 1: non-perennial}. If $|IPR| \leq 0.5$, the binary intermittence class of the reach associated with the gauging station was accurately predicted, with |IPR| values closer to 0.5 indicating greater uncertainty. If IPR > 0.5, the reach was predicted to be non-perennial when it was perennial. If IPR < -0.5, the reach was predicted to be perennial when it was non-perennial. We also examined the distribution of classification accuracy and bias (**Fig. 3)**, as well as residual spatial autocorrelation (see Supplementary Information *Section IV.d*), by river basin.

(iii) Partial dependence plots were generated for the 27 most important predictors using the *edarf* package[89] (see Supplementary Information **Fig. S5**). These plots display estimates of the marginal relationship between each predictor variable and the model's predictions by holding the rest of the predictors at their respective mean values[90].

Assessing the global prevalence of IRES

After training the two final probability RF sub-models, the constructed prediction rules were used to estimate the probability of intermittence for each river reach included in

the global river network (i.e., with MAF ≥ 0.1 $m^3 s^{-1}$). All reaches with a resulting probability ≥ 0.5 were classified to be non-perennial (and perennial otherwise). This threshold was chosen following an analysis of model performance sensitivity to probability thresholds ranging from 0.25 to 0.75 for each RF sub-model which showed a balanced model performance at 0.5 (see Supplementary Information *Section IV.e*). When adjusting the probability threshold between 0.45 and 0.55, the RF-predicted (i.e., non-extrapolated) global prevalence of IRES varied from 36% to 48% (compared to 41% with a 0.5 threshold).

We then used the binary intermittence class predictions to compute the global prevalence of IRES by country, continent, climate zone, terrestrial biome, and major freshwater habitat type (**Table 1** and **Supplementary Data**). Although gauging stations on reaches with MAF < 0.1 $m^3 s^{-1}$ were included in the training dataset, we did not produce RF predictions of the probability of flow intermittence for individual reaches below this discharge threshold for two reasons. First, there existed only 59 gauges with MAF < 0.1 $m^3 s^{-1}$ and at least 10 valid years of data (including only 13 on perennial reaches), which was insufficient to confidently train a model and assess its uncertainty for this discharge size class. Second, there exists a discontinuity in RiverATLAS below 0.1 $m^3 s^{-1}$ whereby only those reaches with a drainage area ≥ 10 km^2 are included[27], leading to a varying discharge cut-off depending on a region's aridity. Bounding our RF predictions to 0.1 $m^3 s^{-1}$ enabled us to establish a robust estimate of the prevalence of flow intermittence in a range of discharge size classes which we then used for an extrapolation to smaller streams (see Methods section *Extrapolating the global prevalence of IRES to smaller streams*).

Estimating human population near IRES

To estimate the percentage of the global population living near an IRES, we first aggregated 2020 population count data from WorldPop[91]. We used constrained, rather than unconstrained, top-down WorldPop population estimates to avoid erroneous allocation of

695 population to all land cells[91]. Population count estimates were aggregated from 3 arc-second
696 (~90 m at the equator) to 15 arc-second pixels (~500 m, i.e., the resolution of the
697 hydrographic data underpinning the RiverATLAS river network). We associated the
698 population within each larger pixel to the river reach in RiverATLAS (with MAF $\geq$ 0.1 m^3 s^{-1}
699) that was nearest to that pixel. Finally, we summed the population across all pixels in the
700 world that were associated with a reach predicted to be non-perennial by our model.

701 **Extrapolating the global prevalence of IRES to smaller streams**

702 To create a first-order approximation of the global prevalence of IRES including even
703 smaller streams, we extrapolated our model estimates to the next smaller streamflow size
704 class range of [0.01, 0.1) m^3 s^{-1}. While streams of this size class are rarely monitored or
705 mapped globally, they are ecologically and environmentally critical[92]. For instance, at least
706 64% of rivers and streams in the U.S. (by length) show a MAF < 0.1 m^3 s^{-1}, and 25% show a
707 MAF < 0.01 m^3 s^{-1} (according to the U.S. National Hydrographic Dataset, NHDPlus at
708 medium resolution). We limited our extrapolation to one order of magnitude (i.e., we did not
709 include even smaller streams, with MAF < 0.01 m^3 s^{-1}, that still can form stream channels) as
710 we expect uncertainties to continuously increase when moving further outside the range of
711 our trained and tested RF model.

712 The prevalence of IRES for this stream size class was independently extrapolated for
713 a total of 465 spatial sub-units representing all occurring intersections of 62 river basin
714 regions (BasinATLAS[27] level 2 subdivisions, average surface area 2.2 x 10^6 km^2) and 18
715 climate zones (Global Environmental Stratification[32]). For each basin-climate sub-unit, we
716 first extrapolated the empirical cumulative distribution of total stream length (of all reaches
717 with MAF $\geq$ 0.1 m^3 s^{-1}) down to 0.01 m^3 s^{-1} MAF using a Generalised Additive Model[93]
718 (GAM). We excluded reaches larger than the 95th percentile of MAF (i.e., the largest rivers)
719 within the sub-unit from model fitting to avoid common discontinuities at the high end of the

empirical distribution that can affect the low end of the power law-like trendline (see Supplementary Information **Fig. S8a&c**).

Second, we extrapolated the prevalence of flow intermittence (in percentage of stream length) down to 0.01 $m^3 s^{-1}$ MAF. In this case, we fitted a GAM for beta-distributed data — i.e., with a (0, 1) range — to the prevalence of intermittence in each logarithmic MAF size bin of the sub-unit. MAF logarithmic size bins ($m^3 s^{-1}$) were defined as $[10^i, 10^{i+0.1})$ for every i in {-1, -0.9, -0.8, …, 5.3} for model fitting, and every i in {-2, -1.9, …, -1.1} for model extrapolation. See Supplementary Information **Fig. S8b&d** for illustrative examples of this approach. GAMs were used to conduct both extrapolations because this non-parametric, non-linear approach does not require assumptions to be made regarding what distribution (e.g., a power-law[94]) the empirical cumulative distributions should follow. This is justifiable because the aim of the analysis was to make a pragmatic first-order approximation of IRES prevalence rather than to demonstrate the existence (or not) of a specific distribution.

Following the fitting of all GAM models, the length of IRES in each linear MAF size class between 0.01 $m^3 s^{-1}$ and 0.1 $m^3 s^{-1}$ was computed as the product of the extrapolated length of streams and the prevalence of intermittence in that size class. Finally, the total length of IRES in the extrapolated size classes was combined with the predictions from the split RF model to estimate the global prevalence of IRES as a percentage of the total global length of rivers and streams with MAF $\geq$ 0.01 $m^3 s^{-1}$.

We also produced an additional estimate with the assumption that, for each basin-climate sub-unit, the prevalence of IRES in streams with 0.01 $\leq$ MAF < 0.1 $m^3 s^{-1}$ was equal to the prevalence of IRES in streams with 0.1 $\leq$ MAF < 0.2 $m^3 s^{-1}$. Even with this conservative assumption, we estimate that 51% of all global rivers and streams with MAF $\geq$ 0.01 $m^3 s^{-1}$ are IRES. In contrast to the RF models, which estimate the probability of flow intermittence at the scale of individual river reaches, the GAM-based extrapolation provides

745 aggregate estimates of IRES prevalence for basin-climate sub-units, which are best suited for
746 global accounting studies.

747 **Model comparisons**

748 *Comparisons with reported intermittence prevalence at national scales*

749 The most common source of information on the prevalence of flow intermittence across
750 large regions are national hydrographic datasets, derived mainly from paper topographic
751 maps in which non-perennial watercourses are usually depicted by dashed lines. We
752 compared our model estimates of the percentage of stream length that is non-perennial with
753 this type of hydrographic data for four countries covering a wide range of environmental,
754 geological, and climatic conditions: the contiguous U.S., Australia, Brazil, and Argentina
755 (**Extended Data Figs. 3-4**; for data sources see **Extended Data Fig. 7b**). In addition, we
756 compared our results in mainland France with predictions of a national model (ref[21]).

757 It should be noted that we do not consider these comparisons to be an accuracy
758 assessment of our model outputs due to the inherent yet unknown uncertainties in the national
759 hydrographic datasets. While the national maps represent the most comprehensive records of
760 presumed intermittence, most are characterized by high levels of inconsistency among
761 regions and cartographers, even for a fixed map scale (e.g., 1:24,000), in both stream density
762 and flow intermittence assessment[95,96]. For instance, streamflow intermittence classifications
763 contained in the U.S. National Hydrography Datasets (NHDPlus, which was used in this
764 study), based on one-time field surveys typically conducted in the mid- to late-1900s, have
765 been shown to exhibit misclassification rates as high as 50% compared to independent field
766 surveys[95,96]. Hafen and colleagues report Only an 80-81% agreement between ground-based
767 streamflow field observations from the U.S. Pacific Northwest and the NHDPlus
768 classifications has been reported (ref[97]). In the Brazilian dataset and the NHDPlus,
769 neighbouring topographic map sheets differ in whether flow intermittence was mapped,

770 leading to artefactual hard edges between regions in terms of the prevalence of
771 intermittence[98] (e.g., **Extended Data Fig. 4**). Despite these limitations, map-based national
772 hydrographic datasets remain the reference used by most government agencies and
773 institutions in determining the extent and flow intermittence of river networks, and thus
774 provide a useful benchmark for comparing the output of our model.

775 A custom processing workflow was developed to format each of the four national river
776 network datasets to ensure comparability with our model predictions. This involved filtering
777 each source dataset to keep only river and stream channels (e.g., excluding lake shorelines
778 and marine coastlines), excluding reaches in the source data that do not correspond with the
779 streamflow threshold applied for the mapped rivers in this study (MAF $\geq$ 0.1 $m^3 s^{-1}$), and
780 excluding artificial channels (e.g., canals and ditches). For a full description of the formatting
781 workflow, see Supplementary Information *Section VI.a*. Following this formatting process,
782 we compared the percentage of river network length that was categorized as IRES in each of
783 the source datasets to our model results for the same region (**Extended Data Fig. 5**). We
784 could not perform this quantitative comparison for Brazil and Argentina because there was no
785 measure of river size in these datasets. Lastly, we visually assessed whether spatial patterns
786 of intermittence were similar between the source datasets and our model results. Aside from
787 Argentina, we were unable to compare our predictions to hydrographic maps in countries
788 where sparse hydrometric networks result in higher modelling uncertainties, due to the
789 unavailability of hydrographic data in these regions.

790 *Comparisons with local on-the-ground visual observations*

791 Datasets of on-the-ground visual observations of flow presence or absence (flow
792 state) by trained individuals provide some of the most reliable records of flow intermittence
793 [22,99,100]. We compared our predictions of intermittence to datasets of this type for two regions:
794 the U.S. Pacific Northwest and mainland France (**Extended Data Fig. 6;** see Supplementary

795 Information *Section VI.b* for additional details). We did not use these observations directly
796 for the training of the RF sub-models as we could not apply the same criterion to define
797 'intermittence' as for gauging stations (i.e., at least one day per year of flow cessation, on
798 average, across the entire record) and their inclusion would have represented a strong
799 regional bias. These datasets instead enabled an independent comparison of the model
800 predictions for smaller rivers and streams (here mostly < 1 $m^3 s^{-1}$), which are poorly
801 represented in the global hydrometric network.

802 For the U.S. Pacific Northwest, we used 5,372 observations across 3,725 reaches
803 (3,547 perennial, 178 non-perennial) from a larger dataset of 24,316 stream observations[101]
804 that occurred from July 1st to October 1st, between 1977 and 2016. The source dataset is a
805 compilation of 11 smaller datasets from independent projects that include aquatic species
806 habitat surveys, wet/dry stream channel mapping, beneficial use reconnaissance surveys, or
807 were collected specifically for the PROSPER intermittent river mapping project[22,101].
808 Streamflow observations included one-time surveys and repeat surveys extending over
809 several years, as well as discrete locations or continuous sections of a stream channel reach.
810 Based on the approach used by Jaeger et al.[22], we considered that a river section was
811 perennial only if all observations (July 1st - October 1st) reported the presence of water.
812 Despite this strict criterion, this dataset may underestimate the prevalence of intermittence
813 since most sites were only observed 1-3 times and the probability that flow cessation is
814 observed at a given reach increased with the number of observations (logistic regression, n =
815 9,850, p-value < 0.001, see Supplementary Information *Section VI.b* for details).

816 For France, we used 124,112 observations across 2,297 reaches (878 perennial, 1,419
817 non-perennial) from a larger set of ca. 3,300 sites uniformly distributed across France from
818 the national river drying observatory (ONDE) network[102]. The ONDE network provides a
819 stable set of sites on river and stream reaches of Strahler orders under five which, since 2012,

have been inspected by agency employees from the French Office for Biodiversity (OFB) at least monthly between May and September. We considered an observation to reflect flow intermittence if it was classified as either "with no visible flow" or "dried out" (as opposed to "with visible flow"). In case of multiple observations on one reach, we considered the reach to be non-perennial if a single observation of flow cessation existed.

All flow state observations were linked to the RiverATLAS stream network through custom semi-automated procedures designed for each dataset, using the proximity between the point observations and the reach locations in RiverATLAS, as well as associated information from local river network datasets and ancillary attribute data provided for each location (e.g., drainage area, site name; see Supplementary Information *Section VI.b* for details). Following data formatting and harmonization, we assessed the degree of agreement at the river reach level between the binary intermittence class predicted by our model and that reported by the two datasets of visual observations.

Methods References

51. Lehner, B. & Grill, G. Global river hydrography and network routing: baseline data and new approaches to study the world's large river systems. *Hydrol. Process.* **27**, 2171–2186 (2013).
52. Lehner, B., Verdin, K. & Jarvis, A. New global hydrography derived from spaceborne elevation data. *Eos, Trans. Am. Geophys. Union* **89**, 93–94 (2008).
53. Messager, M. L., Lehner, B., Grill, G., Nedeva, I. & Schmitt, O. Estimating the volume and age of water stored in global lakes using a geo-statistical approach. *Nat. Commun.* **7**, (2016).
54. Global Runoff Data Centre. In-situ river discharge data. (2015).
55. Do, H. X., Gudmundsson, L., Leonard, M. & Westra, S. The Global Streamflow Indices and Metadata Archive (GSIM) – Part 1: The production of a daily streamflow archive and metadata. *Earth Syst. Sci. Data* **10**, 765–785 (2018).
56. Gudmundsson, L., Do, H. X., Leonard, M. & Westra, S. The Global Streamflow Indices and Metadata Archive (GSIM) – Part 2: Quality control, time-series indices and homogeneity assessment. *Earth Syst. Sci. Data* **10**, 787–804 (2018).
57. Lehner, B. *et al.* High□resolution mapping of the world's reservoirs and dams for sustainable river□ flow management. *Front. Ecol. Environ.* **9**, 494–502 (2011).
58. Mackay, S. J., Arthington, A. H. & James, C. S. Classification and comparison of natural and altered flow regimes to support an Australian trial of the Ecological Limits of Hydrologic Alteration framework. *Ecohydrology* **7**, Wheeler, K., Wenger, S. J., Freeman, M. C. (2018 (2014).
59. Zhang, Y., Zhai, X., Shao, Q. & Yan, Z. Assessing temporal and spatial alterations of flow regimes in the regulated Huai River Basin, China. *J. Hydrol.* **529**, 384–397 (2015).
60. Reynolds, L. V., Shafroth, P. B. & LeRoy Poff, N. Modeled intermittency risk for small streams in the Upper Colorado River Basin under climate change. *J. Hydrol.* **523**, 768–780 (2015).
61. Costigan, K. H. *et al.* Flow regimes in intermittent rivers and ephemeral streams. in *Intermittent Rivers and Ephemeral Streams: Ecology and Management* 51–78 (Academic Press, 2017). doi:10.1016/B978-0-12-803835-2.00003-6.
62. Pickens, A. H. *et al.* Mapping and sampling to characterize global inland water dynamics from 1999 to 2018 with full Landsat time-series. *Remote Sens. Environ.* **243**, 111792 (2020).
63. Hengl, T. *et al.* SoilGrids250m: Global gridded soil information based on machine learning. *PLoS One* **12**, e0169748 (2017).
64. Fick, S. E. & Hijmans, R. J. WorldClim 2: new 1-km spatial resolution climate surfaces for global land areas. *Int. J. Climatol.* **37**, 4302–4315 (2017).
65. Trabucco, A. & Zomer, R. Global Aridity Index and Potential Evapotranspiration (ET0) Climate Database v2. (2018) doi:10.6084/m9.figshare.7504448.v1.
66. Bond, N. R. & Kennard, M. J. Prediction of hydrologic characteristics for ungauged catchments to support hydroecological modeling. *Water Resour. Res.* **53**, 8781–8794 (2017).
67. Kotsiantis, S. B., Zaharakis, I. D. & Pintelas, P. E. Machine learning: A review of classification and combining techniques. *Artif. Intell. Rev.* **26**, 159–190 (2006).
68. Wainer, J. Comparison of 14 different families of classification algorithms on 115 binary datasets. *arXiv:1606.00930* (2016).
69. Malley, J. D., Kruppa, J., Dasgupta, A., Malley, K. G. & Ziegler, A. Probability Machines. *Methods Inf. Med.* **51**, 74–81 (2012).
70. Wright, M. N. & Ziegler, A. ranger : A fast implementation of random forests for high dimensional data in C++ and R. *J. Stat. Softw.* **77**, (2017).
71. Lang, M. *et al.* mlr3: A modern object-oriented machine learning framework in R. *J. Open Source Softw.* **4**, 1903 (2019).
72. Landau, W. M. The drake R package: a pipeline toolkit for reproducibility and high-performance computing. *J. Open Source Softw.* **3**, 550 (2018).
73. Hothorn, T., Hornik, K. & Zeileis, A. Unbiased recursive partitioning: A conditional inference framework. *J. Comput. Graph. Stat.* **15**, 651–674 (2006).
74. Hothorn, T. & Zeileis, A. Partykit: A modular toolkit for recursive partytioning in R. *J. Mach. Learn. Res.* **16**, 3905–3909 (2015).
75. Wright, M. N., Dankowski, T. & Ziegler, A. Unbiased split variable selection for random survival forests using maximally selected rank statistics. *Stat. Med.* **36**, 1272–1284 (2017).
76. Zhang, G. & Lu, Y. Bias-corrected random forests in regression. *J. Appl. Stat.* **39**, 151–160 (2012).
77. Japkowicz, N. & Stephen, S. The class imbalance problem: A systematic study. *Intell. Data Anal.* **6**, 429–449 (2002).
78. Bischl, B., Mersmann, O., Trautmann, H. & Weihs, C. Resampling methods for meta-model validation with recommendations for evolutionary computation. *Evol. Comput.* **20**, 249–275 (2012).

79. Probst, P., Wright, M. N. & Boulesteix, A. L. Hyperparameters and tuning strategies for random forest. *Wiley Interdiscip. Rev. Data Min. Knowl. Discov.* **9**, e1301 (2019).
80. Probst, P. & Boulesteix, A. L. To tune or not to tune the number of trees in random forest. *J. Mach. Learn. Res.* **18**, 1–8 (2018).
81. Schratz, P., Muenchow, J., Iturritxa, E., Richter, J. & Brenning, A. Hyperparameter tuning and performance assessment of statistical and machine-learning algorithms using spatial data. *Ecol. Modell.* **406**, 109–120 (2019).
82. Brenning, A. Spatial cross-validation and bootstrap for the assessment of prediction rules in remote sensing: The R package sperrorest. in *International Geoscience and Remote Sensing Symposium (IGARSS)* 5372–5375 (2012). doi:10.1109/IGARSS.2012.6352393.
83. Meyer, H., Reudenbach, C., Hengl, T., Katurji, M. & Nauss, T. Improving performance of spatio-temporal machine learning models using forward feature selection and target-oriented validation. *Environ. Model. Softw.* **101**, 1–9 (2018).
84. Meyer, H., Reudenbach, C., Wöllauer, S. & Nauss, T. Importance of spatial predictor variable selection in machine learning applications – Moving from data reproduction to spatial prediction. *Ecol. Modell.* **411**, (2019).
85. Brodersen, K. H., Ong, C. S., Stephan, K. E. & Buhmann, J. M. The balanced accuracy and its posterior distribution. in *Proceedings - International Conference on Pattern Recognition* 3121–3124 (2010). doi:10.1109/ICPR.2010.764.
86. Altmann, A., Toloşi, L., Sander, O. & Lengauer, T. Permutation importance: a corrected feature importance measure. *Bioinformatics* **26**, 1340–1347 (2010).
87. Amaratunga, D., Cabrera, J. & Lee, Y.-S. Enriched random forests. *Bioinformatics* **24**, 2010–2014 (2008).
88. Evans, J. S., Murphy, M. A., Holden, Z. A. & Cushman, S. A. Modeling species distribution and change using random forest. in *Predictive Species and Habitat Modeling in Landscape Ecology: Concepts and Applications* 139–159 (Springer New York, 2011). doi:10.1007/978-1-4419-7390-0_8.
89. Jones, Z. M. & Linder, F. J. edarf: Exploratory Data Analysis using Random Forests. *J. Open Source Softw.* **1**, 92 (2016).
90. Friedman, J. H. Greedy function approximation: A gradient boosting machine. *Ann. Stat.* **29**, 1189–1232 (2001).
91. Bondarenko, M., Kerr, D., Sorichetta, A. & Tatem, A. J. Census/projection-disaggregated gridded population datasets for 189 countries in 2020 using Built-Settlement Growth Model (BSGM) outputs. (2020) doi:10.5258/SOTON/WP00684.
92. Colvin, S. A. R. *et al.* Headwater streams and wetlands are critical for sustaining fish, fisheries, and ecosystem services. *Fisheries* **44**, 73–91 (2019).
93. Hastie, T., Tibshirani, R. & Friedman, J. *The elements of statistical learning: data mining, inference, and prediction*. (Springer Science & Business Media, 2009).
94. Clauset, A., Shalizi, C. R. & Newman, M. E. J. Power-law distributions in empirical data. *SIAM Rev.* **51**, 661–703 (2009).
95. Fritz, K. M. *et al.* Comparing the extent and permanence of headwater streams from two field surveys to values from hydrographic databases and maps. *J. Am. Water Resour. Assoc.* **49**, 867–882 (2013).
96. Stoddard, J. L. *et al. Environmental Monitoring and Assessment Program (EMAP): western streams and rivers statistical summary*. *EPA/620/R-05/006 (NTIS PB2007-102088)* (2005).
97. Hafen, K. C., Blasch, K. W., Rea, A., Sando, R. & Gessler, P. E. The Influence of Climate Variability on the Accuracy of NHD Perennial and Nonperennial Stream Classifications. *JAWRA J. Am. Water Resour. Assoc.* **56**, 903–916 (2020).
98. Colson, T., Gregory, J., Dorney, J. & Russell, P. Topographic and soil maps do not accurately depict headwater stream networks. *Natl. Wetl. Newsl.* **30**, 25–28 (2008).
99. Alderman, K., Turner, L. R. & Tong, S. Floods and human health: A systematic review. *Environ. Int.* **47**, 37–47 (2012).
100. Datry, T., Pella, H., Leigh, C., Bonada, N. & Hugueny, B. A landscape approach to advance intermittent river ecology. *Freshw. Biol.* **61**, 1200–1213 (2016).
101. McShane, R. R., Sando, R. & Hockman-Wert, D. P. Streamflow observation points in the Pacific Northwest, 1977-2016. *U.S. Geological Survey data release* https://www.sciencebase.gov/vocab/category/item/identifier (2017) doi:10.5066/F7BV7FSP.
102. Nowak, C. & Durozoi, B. *ONDE: Guide de dimensionnement et de mise en oeuvre du suivi national des étiages estivaux*. http://reseau.eaufrance.fr/webfm_send/4297 (2014).
103. Busch, M. H. *et al.* What's in a Name? Patterns, Trends, and Suggestions for Defining Non-Perennial Rivers and Streams. *Water* **12**, 1980 (2020).
104. Datry, T. *et al.* Science and Management of Intermittent Rivers and Ephemeral Streams (SMIRES). *Res.*

Ideas Outcomes **3**, e21774 (2017).
105. Trabucco, A. & Zomer, R. J. Global Soil Water Balance Geospatial Database. (2010) doi:10.6084/m9.figshare.7707605.v3.
106. Hall, D. K. & Riggs, G. A. MODIS/Aqua Snow Cover Daily L3 Global 500m SIN Grid, Version 6. [2002-2015]. (2016).
107. Fan, Y., Li, H. & Miguez-Macho, G. Global Patterns of Groundwater Table Depth. *Science* **339**, 940–943 (2013).
108. Fluet-Chouinard, E., Lehner, B., Rebelo, L.-M., Papa, F. & Hamilton, S. K. Development of a global inundation map at high spatial resolution from topographic downscaling of coarse-scale remote sensing data. *Remote Sens. Environ.* **158**, 348–361 (2015).
109. Döll, P., Kaspar, F. & Lehner, B. A global hydrological model for deriving water availability indicators: model tuning and validation. *J. Hydrol.* **270**, 105–134 (2003).
110. Bartholomé, E. & Belward, A. S. GLC2000: a new approach to global land cover mapping from Earth observation data. *Int. J. Remote Sens.* **26**, 1959–1977 (2005).
111. GLIMS and National Snow and Ice Data Center. GLIMS Glacier Database, V1. (2012) doi:http://dx.doi.org/10.7265/N5V98602.
112. Gruber, S. Derivation and analysis of a high-resolution estimate of global permafrost zonation. *Cryosph.* **6**, 221–233 (2012).
113. Ramankutty, N. & Foley, J. A. Estimating historical changes in global land cover: Croplands from 1700 to 1992. *Global Biogeochem. Cycles* **13**, 997–1027 (1999).
114. Lehner, B. & Döll, P. Development and validation of a global database of lakes, reservoirs and wetlands. *J. Hydrol.* **296**, 1–22 (2004).
115. Robinson, N., Regetz, J. & Guralnick, R. P. EarthEnv-DEM90: A nearly-global, void-free, multi-scale smoothed, 90m digital elevation model from fused ASTER and SRTM data. *ISPRS J. Photogramm. Remote Sens.* **87**, 57–67 (2014).
116. Williams, P. W. & Ford, D. C. Global distribution of carbonate rocks. *Zeitschrift Fur Geomorphol. Suppl.* **147**, 1 (2006).
117. Hartmann, J. & Moosdorf, N. The new global lithological map database GLiM: A representation of rock properties at the Earth surface. *Geochemistry, Geophys. Geosystems* **13**, (2012).

Data availability

The global river network dataset and the associated attribute information for every river reach—that is, the hydro-environmental attributes, predicted probability of intermittence and associated binary class —as well as the main results of the study are available at https://figshare.com/s/a60b0c16b93738f2bbc0T [*will be replaced with DOI upon final acceptance of the manuscript*]. The dataset can be used together with the published source code (see 'Code availability') to recalculate the main study results with updated data and parameters. The streamflow time series from the Global Runoff Data Centre are available in summarized format. The daily records are not available in the data repository owing to licensing issues but are freely available upon written request through https://www.bafg.de/GRDC/EN/Home/homepage_node.html. Original data that supported the study are freely available and their sources are summarized in **Extended Data Fig. 7b**.

Code availability

The source code and results of this research are available under the GNU General Public License v3.0 at https://messamat.github.io/globalIRmap/.

Acknowledgement

We thank Dr. Tim Elrick and the Geographic Information Centre at McGill University for providing us with high-performance computing resources. Funding for this study was provided in part by the Natural Sciences and Engineering Research Council of Canada (BL, CC, CW, MLM, NSERC Discovery Grants RGPIN/341992-2013 and RGPIN/04541-2019); McGill University (MLM, Tomlinson Fellowship), Montreal, Quebec, Canada; H_2O'Lyon Doctoral School (MLM, Doctoral Fellowship, ANR-17-EURE-0018), Lyon, France; TD, NL, HP and TT were supported by the DRYvER project (http://www.dryver.eu/), which has received funding from the European Union's Horizon 2020 research and innovation programme under grant agreement No. 869226.

Author contributions

CRediT (Contributor Roles Taxonomy): conceptualization - TD, BL, KT, MLM; Methodology - MLM, BL, TS, CC, NL; data curation - MLM, BL, CC, CW, TS, HP; software, validation, visualization - MLM; formal analysis - MLM, CC; writing original draft - MLM, TD, BL; writing review and editing - all authors; project administration and supervision - MLM, BL, TD; funding acquisition - BL, TD, MLM.

Competing interests

The authors declare no competing interests.

Additional information

Correspondence and requests for materials should be addressed to Mathis L. Messager (mathis.messager@mail.mcgill.ca).

Extended Data legends

Extended Data Table 1 | Definitions of commonly used terms for non-perennial rivers and streams.

Extended Data Table 2 | Hydro-environmental characteristics used as candidate predictor variables in the split random forest model. Spatial representations refer to: *p* (derived at the pour point of the river reach), *c* (derived within the local catchment that drains directly into the reach), or *u* (derived within the total drainage area upstream of reach pour point). See ref[27] for a full description of the methodology to calculate the variables.

Extended Data Fig. 1 | Global prevalence of IRES with at least one zero-flow month per year on average. a, Distribution of global climate zones used in this study. Data provided by Global Environmental Stratification (GEnS[32]). **b**, Predicted probability of river flow intermittence, defined as at least one zero-flow month (30 days) per year on average, across the global river and stream network[27]. The median probability threshold of 0.5 was used to determine the binary flow intermittence class for each reach. **c**, Global prevalence of IRES with at least one zero-flow month (30 days) per year on average, across climate zones and streamflow size classes (based on long-term average naturalised discharge). Note that in regions with sparse training data, the model results can differ substantially from the results shown in Table 1, as the underlying random forest and extrapolation models were developed independently. No stations were available in the Arctic (1 & 2), and few stations were available in Extremely cold and wet (1 & 2) and in Extremely hot and arid climates (together representing 3% of global river and stream length). Rows are sorted in the same order as in Table 1, and the same footnotes as in Table 1 apply. Mapping software: ArcMap™ (ESRI).

Extended Data Fig. 2 | Distribution of cross-validation results. a, Maps of spatially cross-validated predictive accuracy of flow intermittence for streamflow gauging stations. See Supplementary Information **Fig. S3** for the distribution of spatial cross-validation folds and details on the cross-validation procedure. The classification errors shown here are not necessarily present in the final predictions but illustrate the ability of the model to predict the flow intermittence class for each region if that region was excluded from the training set. For instance, it shows that the model would be unable to predict the presence of IRES in western France and northern Spain (inset *ii*, dark red dots), or in western India (inset *iii*) without training stations in these regions. **b-e**, Intermittence prediction residuals vs. gauging station characteristics and environmental variables. The mean intermittence prediction residual (IPR) is the difference between the average predicted probability of flow intermittence (across 3 cross-validation folds and 2 repetitions) and the observed flow intermittence of the gauging station (1 = non-perennial, 0 = perennial). Overall, prediction errors and uncertainties decrease with an increase in the number of recorded years by gauging stations as well as the drainage area and the degree of flow intermittence (average annual number of zero-flow days and flow cessation events) of the corresponding reaches. Mapping software: ArcMap™ (ESRI).

Extended Data Table 3 | Performance summary of binary flow intermittence class predictions. Tables show summary results for the split model approach based on **a**, a twice-repeated 3-fold non-spatial cross-validation (CV) and **b**, a once-repeated 40-fold spatial CV, as well as for comparison **c**, a single (non-split) model approach based on a twice-repeated 3-fold non-spatial CV. The color coding mirrors Extended Data Fig. 2 with light colors slightly

darkened for readability. The split model approach involves training two random forest sub-models with slightly overlapping MAF ranges, one trained to predict the streamflow intermittence probability of small-to-medium rivers with MAF < 10 $m^3 s^{-1}$ and the other for medium-to-large rivers with MAF ≥ 1 $m^3 s\text{-}^{1}$. Within the overlapping range of 1-10 $m^3 s^{-1}$ MAF, the average probability was calculated to avoid abrupt transitions at a singular size threshold. Gauging stations monitoring streams with a mean annual naturalised discharge < 0.1 $m^3 s^{-1}$ were included in model training and testing (shown in grey font); however, no model predictions were made below this discharge threshold. Sensitivity is the proportion of non-perennial reaches correctly classified as non-perennial. Specificity is the proportion of perennial reaches correctly classified as perennial. Precision is the proportion of reaches classified as non-perennial that are truly non-perennial. See Supplementary Information **Fig. S3** and *Section IV.b* for the distribution of spatial cross-validation folds and details on the cross-validation procedure.

Extended Data Fig. 3 | Comparing global predictions to national maps of IRES in the U.S. and Australia. Comparison of **a**, the U.S. National Hydrographic Dataset (NHDPlus, medium resolution) and **d**, the Australian hydrological geospatial fabric, with our model predictions based on two thresholds of flow intermittence, either **b, e,** ≥ 1 zero-flow day per year or **c, f**, ≥ 1 zero-flow month (30 days) per year, on average. Only rivers and streams with MAF ≥ 0.1 $m^3 s^{-1}$ are shown for the U.S. (**a-c**) and with drainage area ≥ 10 km^2 for Australia (**d-f**). The U.S. reference dataset portrays 19-22% of the length of rivers and streams as non-perennial, depending on whether reaches without flow intermittence status are assumed to be perennial or removed; our estimates range from 51% (≥ 1 zero-flow day per year) to 36% (≥ 1 zero-flow month per year). We hypothesize that the remaining gap in IRES prevalence is attributable to a tendency of our model to overpredict intermittence across the eastern U.S and an under-accounting of intermittence in medium to large rivers by the national dataset. The Australian reference dataset portrays 91% of the length of rivers and streams as non-perennial; our estimates range from 95% (≥ 1 zero-flow day per year) to 92% (≥ 1 zero-flow month per year). See Extended Data Fig. 7b for data sources. Mapping software: ArcMap™ (ESRI).

Extended Data Fig. 4 | Comparing global predictions to national maps of IRES in Brazil, Argentina, and France. Comparison of **a**, the continuous cartographic base of Brazil (BC250), **d**, the Argentinian hydrographic network, and **g**, model predictions from Snelder et al. (2013), with our model predictions based on two thresholds of flow intermittence, either **b, e, h,** ≥ 1 zero-flow day per year or **c, f**, ≥ 1 zero-flow month (30 days) per year, on average. In **a** and **d**, only first-order streams (determined through network analysis) are visually differentiated (finer, semi-transparent lines) due to the lack of watercourse size attribute in the Brazilian and Argentinian datasets. In **b-c, e-f, and g-h**, only rivers and streams with MAF ≥ 0.1 $m^3 s^{-1}$ are shown. Snelder et al. predict that 17% of the length of rivers and streams in France are non-perennial. We predict that 14% are non-perennial. This slight divergence may be partly driven by the difference in definition of flow intermittence: Snelder et al. classified stations with ≥ 1 zero-flow day in the streamflow record as IRES whereas we used a threshold of 1 zero-flow day per year across the streamflow record. See Extended Data Fig. 7b for data sources. Mapping software: ArcMap™ (ESRI).

Extended Data Fig. 5 | Quantitative comparison between the predicted prevalence of flow intermittence and national estimates. Comparisons were conducted for France (**a-b**), the U.S. (**c-d**), and Australia (**e-f**), based on two thresholds of flow intermittence, either (**a, c,**

e) ≥ 1 zero-flow day per year or (**b, d, f**) ≥ 1 zero-flow month (30 days) per year, on average. Bars for mapped rivers and streams with MAF < 0.1 $m^3 s^{-1}$ (for France and the U.S.) are greyed-out as they were not included in the calculation of summary statistics. Inset graphs in **b, d, f** show comparisons of total river network length (log-transformed y-axis), which in case of discrepancies can explain some of the differences in the predicted prevalence of intermittence.

Extended Data Fig. 6 | Comparing global predictions to on-the-ground observations of flow cessation. Maps show individual RiverATLAS reaches and their predictive accuracy for **a**, France and **b**, the U.S. Pacific Northwest. Maps are drawn at identical cartographic scales. France (n=2,297): balanced accuracy=0.59, classification accuracy=51%, sensitivity=24%, specificity=94%. U.S. Pacific Northwest (n=3,725): balanced accuracy=0.47, classification accuracy=80%, sensitivity=10%, specificity=83%. See Extended Data Fig. 7b for data sources. Mapping software: ArcMap™ (ESRI).

Extended Data Fig. 7 | Overview of study design and main data sources. a, Diagram of modelling workflow and **b**, main data sources used in model development, predictions, diagnostics, and comparisons.

Extended Data Fig. 8 | Spatial and environmental distribution of streamflow gauging stations used in model training and cross-validation. Gauging stations (n = 5,615) were deemed **a,** perennial if their streamflow record included less than one zero-flow day per year, on average, across their record, or **b,** non-perennial if they included at least one zero-flow day per year, on average, and at least one zero-flow day in every 20-year moving window across their record. Stations fulfilling neither condition a nor b were excluded. Darker points symbolize longer streamflow records. Only gauging stations with streamflow time series spanning at least 10 years were included in this analysis, excluding years with more than 20 missing days. **c-p.** Distribution of values for 14 hydro-environmental variables across the streamflow gauging stations used for model training/testing (purple, n = 5,615) and across all reaches of the global river network (blue, n = 23.3 x 10^6). The distribution plots show empirical probability density functions (i.e., the area under each density function is equal to one) for all variables, aside from Climate Zones (**g**) for which the relative frequency distribution is shown. All variables were averaged across the total drainage area upstream of the reach pour point associated with each gauging station or river reach, respectively. See Extended Data Table 2 for a description of the variables and Extended Data Fig. 1a for a description of the climate zones. No stations were available for climate zones Arctic 1 and Arctic 2. Mapping software: R statistical software (R Core Team).

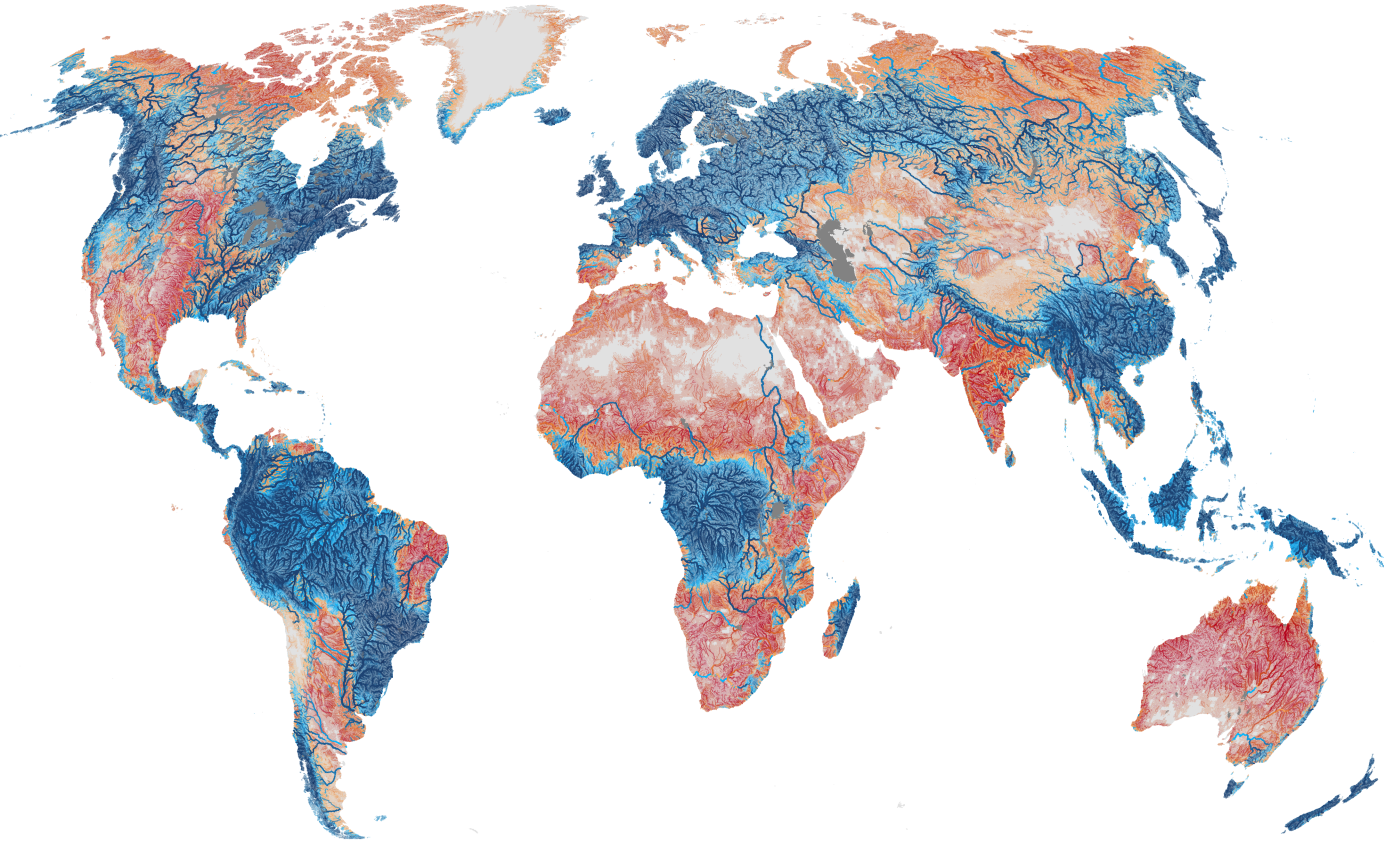
Mean annual discharge
(line width and transparency)
10^{-1} 1 10 10^{2} 10^{3} 10^{4} $m^3 s^{-1}$
Probability of flow intermittence
Non-perennial
Perennial
1 0.75 0.5 0.25 0
Lake or reservoir
No flow

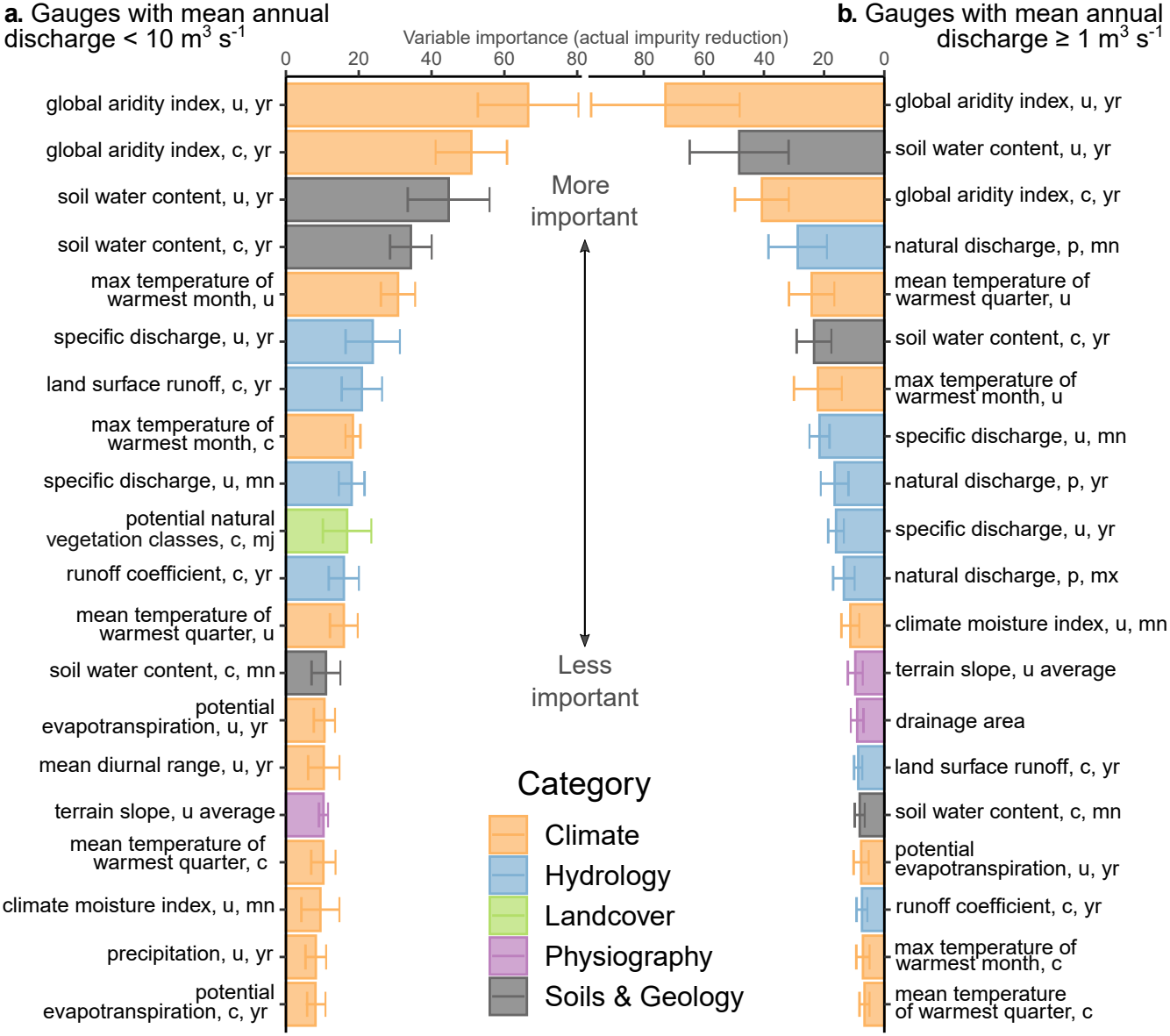
a. Gauges with mean annual discharge < 10 m3 s-1
b. Gauges with mean annual discharge ≥ 1 m3 s-1
Variable importance (actual impurity reduction)
0
20
40
60
80
More important
Less important
global aridity index, u, yr
global aridity index, c, yr
soil water content, u, yr
soil water content, c, yr
max temperature of warmest month, u
specific discharge, u, yr
land surface runoff, c, yr
max temperature of warmest month, c
specific discharge, u, mn
potential natural vegetation classes, c, mj
runoff coefficient, c, yr
mean temperature of warmest quarter, u
soil water content, c, mn
potential evapotranspiration, u, yr
mean diurnal range, u, yr
terrain slope, u average
mean temperature of warmest quarter, c
climate moisture index, u, mn
precipitation, u, yr
potential evapotranspiration, c, yr
global aridity index, u, yr
soil water content, u, yr
global aridity index, c, yr
natural discharge, p, mn
mean temperature of warmest quarter, u
soil water content, c, yr
max temperature of warmest month, u
specific discharge, u, mn
natural discharge, p, yr
specific discharge, u, yr
natural discharge, p, mx
climate moisture index, u, mn
terrain slope, u average
drainage area
land surface runoff, c, yr
soil water content, c, mn
potential evapotranspiration, u, yr
runoff coefficient, c, yr
max temperature of warmest month, c
mean temperature of warmest quarter, c
Category
Climate
Hydrology
Landcover
Physiography
Soils & Geology

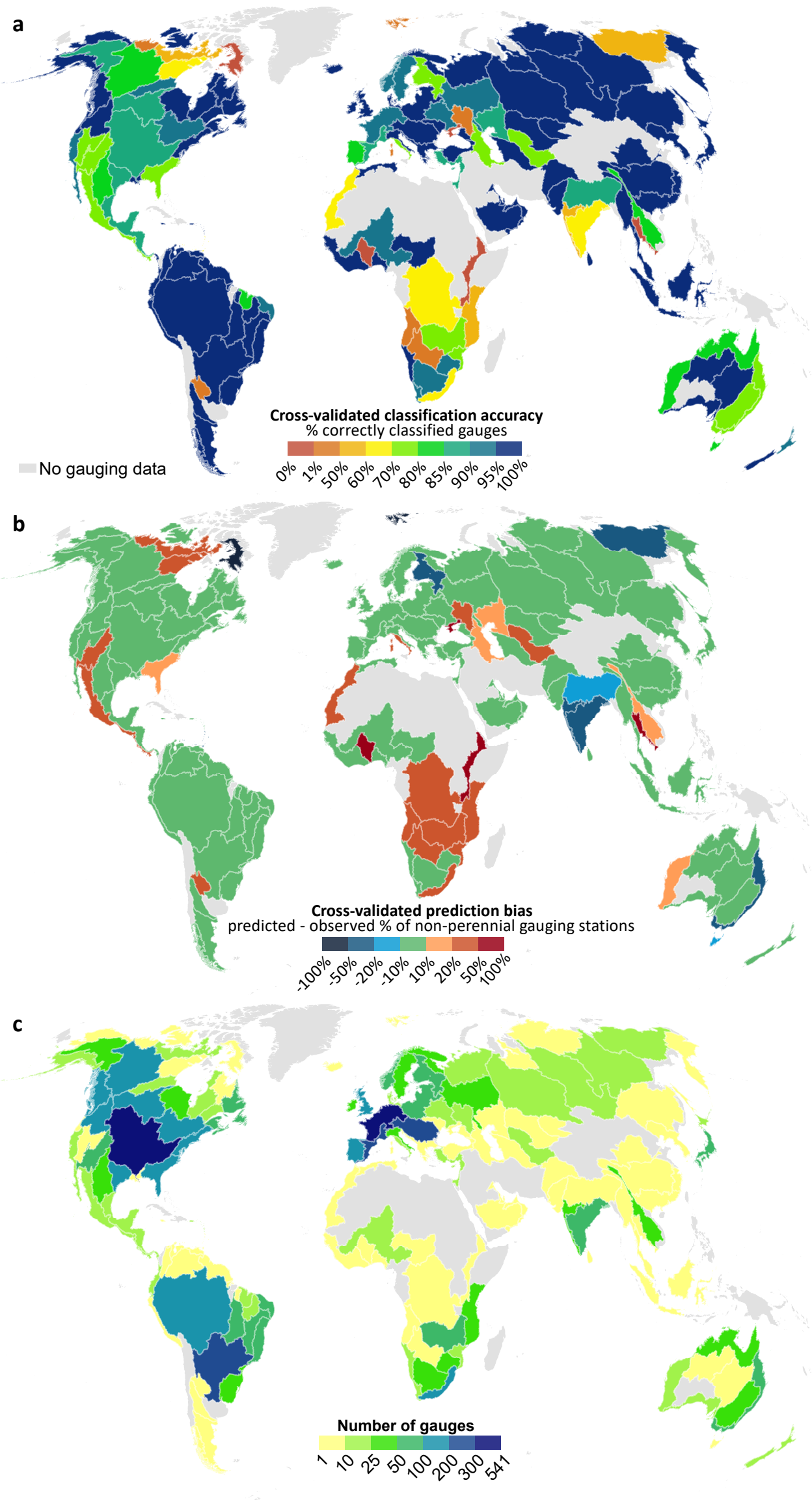
a
Cross-validated classification accuracy
% correctly classified gauges
0%
1%
50%
60%
70%
80%
85%
90%
95%
100%
No gauging data
b
Cross-validated prediction bias
predicted - observed % of non-perennial gauging stations
-100%
-50%
-20%
-10%
10%
20%
50%
100%
c
Number of gauges
1
10
25
50
100
200
300
541